3A.5

BULK MICROPHYSICAL VARIABILITY OF THUNDERSTORMS IN DIFFERENT CLIMATIC REGIONS: COMPARATIVE PREDICTIVE SKILLS OF MELTING LEVEL, CLOUD BASE TEMPERATURE AND CLOUD BASE PRESSURE IN A THREE-DIMENSIONAL NUMERICAL MODELING STUDY

Robert E. Schlesinger and Pao K. Wang
Department of Atmospheric and Oceanic Sciences
University of Wisconsin – Madison
Madison, Wisconsin 53706
USA

1. INTRODUCTION

A succession of research groups at the University of Wisconsin, led by second author Wang, has for over 20 years been studying the microphysical structure of thunderstorms as documented in Straka (1989), Johnson et al. (1993, 1994), Lin and Wang (1997), Lin et al. (2005, henceforth LWS05) and Schlesinger et al. (2006, henceforth SHW06; 2008, henceforth SHW08). The key tool has been the three-dimensional (3D) cloud model WISCDYMM (Wisconsin Dynamical and Microphysical Model), originated by Straka (1989) and subsequently modified by Johnson et al. (1993, 1994), Lin and Wang (1997), LWS05 and SHW06.

By means of six 2-h WISCDYMM simulations, LWS05 compared the microphysical aspects of three summertime thunderstorms apiece in two contrasting climatic regions, the US High Plains (one case each from Colorado, Montana and North Dakota) and the humid subtropics (one case from Taipei, Taiwan and two south Florida cases). Despite being limited to only two climatic regions and one season of the year, LWS05 yielded two notable findings:

a) Throughout the active life of a given storm after its early adjustment phases, the fraction of the total condensate mass contributed by each hydrometeor type seemed to be quasi-steady, along with the individual microphysical transfer rates contributing to the production and depletion of each precipitating hydrometeor category; and

b) The partitioning broke down differently in one region versus the other. The High Plains storms had much higher ice (total frozen condensate) mass fractions than the subtropical storms, ~0.78-0.82 versus ~0.48-0.57. Since the simulated storm structures were found to compare favorably with observations (LWS05), it is quite plausible to regard them as physically realistic.

**Corresponding author address:* Robert E. Schlesinger, Department of Atmospheric and Oceanic Sciences, University of Wisconsin - Madison, Madison, Wisconsin, 53706; e-mail: schlesin@meteor.wisc.edu.

The above findings motivated us to embark on a WISCDYMM-based thunderstorm variability study in the same spirit as in LWS05, but far larger in scope. This expanded study, as reported in SHW08, subsumes 105 thunderstorm cases distributed among 10 climatic zones, including nearly 40 cases from seasons other than summer.

This substantially wider thunderstorm variability study, of which an earlier stage with 56 cases distributed among the same 10 climatic zones was reported in SHW06, was compiled in order to investigate whether systematic differences in the bulk microphysics of simulated storms in contrasting climatic regions continue to apply as markedly as in LWS05 when the variety of thunderstorm-supporting environments is thus broadened.

As reported in SHW08, such did not turn out to be the case. For both the full set of 105 simulations and a subset of 64 limited to the warm months, taken to be May-September in the Northern Hemisphere and November-March in the Southern Hemisphere, all of the four best-sampled climate zones (temperate continental with warm summers, humid subtropical, Mediterranean, humid tropical) showed wide intrazonal spreads in the ice mass fraction, well over half the total range of ~0.20-0.80 for the entire storm population. Also, the mean ice fraction were comparable in all of the first three zones, between ~0.59 and ~0.65. The mean ice fraction was indeed higher for the locations with "High Plains" characteristics (semi-arid and extratropical with at least 700 m MSL surface elevation) but only modestly so (~0.7) versus the humid subtropics (~0.6), although far lower for the humid tropics (~0.45).

In light of the above findings, and the general tendency for cool-season extratropical thunderstorms to occur in air masses substantially warmer and/or moister than "climatology", SHW08 departed from LWS05 by focusing on using linear regression analysis to evaluate correlations between the WISCDYMM-derived hydrometeor mass fractions (HMF's) and environmental indices that can be computed from the initial model sounding. In particular, SHW08 evaluated the ground-relative melting level (ZMLT) both as sole predictor and jointly with the Convective Available Potential Energy

(CAPE), which is also among the key parameters in the context of severe storm forecasting.

As reported in SHW08, for both the full and warm-month storm case populations, the univariate analyses of the HMF's versus ZMLT alone yielded fair negative correlations between ~ -0.44 and ~ -0.48 versus the (total) ice and cloud ice, and somewhat better positive correlations of ~ 0,60 versus rain. But more strikingly, the bivariate analyses with CAPE added as the second predictor boosted the correlation magnitudes substantially for both of the frozen HMF's, to between ~0.64 and ~0.69, and less markedly but still appreciably for rain, to ~0.72 (no meaningful sign can be attached to a multiivariate correlation coefficient). Each of the other three HMF's under consideration (hail, snow, cloud water) yielded weaker correlations than those just mentioned, especially for cloud water, but each bivariate regression analysis again outperformed its univariate counterpart.

We have since built upon the work reported in SHW08 by applying the same univariate and bivariate analysis techniques as we used for the melting level in that paper, but using the cloud-base temperature and cloud-base pressure as alternate primary predictors for the HMF's. This paper highlights the results from our further statistical analyses for the same suite of WISCDYMM storm simulations, using the results from SHW08 as a benchmark of comparison.

2. SUMMARY OF RELEVANT MODEL ASPECTS

2.1 *Model Properties*

WISCDYMM is a time-dependent nonhydrostatic quasi-compressible 3D model on a Cartesian Arakawa-C staggered grid. The model domain is 55x55x20 km^3 in the respective x-, y- and z-coordinates, with uniform grid cell dimensions of 1.0x1.0x0.2 km^3. Finite-difference advection schemes and boundary conditions are as in LWS05, with subgrid flux parameterizations as in Straka (1989). Radiation, topography and the Coriolis force are omitted. The time step is 2 s with a reduced sound speed of 200 m s^{-1}, running each simulation out to 2 h.

The microphysical package in WISCDYMM admits five classes of hydrometeors: cloud water, cloud ice, rain, snow and graupel/hail. It features a bulk parameterization which, as elaborated in Straka (1989), is based mainly on Lin et al. (1983) and Cotton et al. (1982, 1986). Cloud water droplets and cloud ice crystals are monodisperse and move with the air, while precipitating hydrometeors follow inverse exponential size distributions.

The bulk microphysics parameterization provides for up to 37 mass transfer rates among water substance classes, although several of these rates (e.g., condensation onto and evaporation from wet snow and wet graupel/hail) are turned off in this study. As itemized in Table 1 of SHW06, 25 of the active transfer rates are a source or sink of precipitation.

Our methodology for selecting storm cases is summarized in section 2.5 of SHW08. For each case, the horizontally homogeneous base-state potential temperature, water vapor mixing ratio and horizontal wind components are derived by vertically interpolating to the model grid levels the closest available sufficiently deep rawinsounding to the observed convective event in space and time, obtained from the University of Wyoming's sounding archive website

http://weather.uwyo.edu/upperair/sounding.html

As in Klemp and Wilhelmson (1978), a quasi-ellipsoidal buoyant bubble is then superimposed in the lower central portion of the model domain. If the resulting model storm is unrealistically weak and/or short-lived, the buoyant impulse is imposed only after preconditioning the base-state temperature and mixing ratio profiles in the interpolated sounding via prescribed limited-duration mesoscale lifting through the depth of the impulse to suitably increase the relative humidities and/or weaken any caps. The details of the model initialization procedure are covered in section 2.2 of SHW08.

Each 2-h WISCDYMM simulation is run in six 20-min save/restart segments, saving the model fields and auxiliary microphysical data every 2 min. The main convective activity is kept well within the domain area by translating the model domain at a suitable earth-relative velocity, constant throughout any one segment but generally varying from one segment to another.

3. RANGE OF CLIMATIC REGIONS SAMPLED

The global map shown in Fig. 1, identical to Fig. 1 of SHW08 but reproduced here for completeness, plots the locations of the 79 stations for which University of Wyoming archive rawinsoundings were processed to define the initial environments in the 105 WISCDYMM storm simulations. Of these locations, 62 entail one case each and the remaining 17 from two to four cases each. About two-thirds of the storm cases are from the United States east of the Rockies, western and central Europe or southeast Asia, with much sparser sampling from other regions that have lower thunderstorm frequencies, poorer rawinsonde coverage or both.

As displayed in detail in Table 1 of SHW08, the 79 sounding stations are grouped by each of 10 climatic zones adapted from Moran and Morgan (1994). Our climatic terminology differs from theirs in that we have subjectively subdivided their "temperate continental" zones into "warm summer" and "cool summer" subtypes and used the common synonym “Mediterranean” for their “dry summer” subtropical zones.

The “High Plains” descriptor in LWS05 is not among the climatic classifications in Moran and Morgan

(1994). Nevertheless, we regard five of the extratropical stations, encompassing seven of the storm cases, as having High Plains characteristics because they occurred at semi-arid locations at or above 700 m MSL. This applies to five cases among four dry/steppe stations and two cases at one boreal station, symbolized in Table 1 of SHW08 by suffixing with "HP" the climatic descriptors for those five stations.

Table 1, identical to Table 2 of SHW08, displays the numerical partitioning of the 79 stations and 105 cases among the 10 climate zones. Clear majorities of both counts are distributed among four of the zones: warm-summer temperate continental, humid subtropical, Mediterranean and humid tropical, each of the remaining six zones being much more sparsely represented for the same reasons as the highly uneven distribution of the station locations in Fig. 1.

In LWS05, all six storm cases occurred in the Northern Hemisphere and were confined to the summer months of June through August. In our current 105-case study, by contrast, excluding three cases within 10˚ of the equator and hence nearly devoid of thermal seasonality, 38 Northern Hemisphere cases occurred outside of the warm months, defined for our purposes as May through September. Also, another 10 of our cases occurred in the Southern Hemisphere, though all of those 10 cases were confined to the corresponding warm months of November through March.

4. LINEAR REGRESSION METHODOLOGY

A WISCDYMM simulation of a real convective storm from the past is akin to numerical weather prediction, albeit strictly in the sense of "hindcasting" and on far smaller spatial and temporal scales than an operational synoptic-scale numerical weather forecast run out to a week or so. However, in the context of both our univariate and bivariate linear regression analyses, we henceforth take each environmental index derived from the processed initial model sounding to be "observed", as we also do for any quantity derived from run-time WISCDYMM output, and we regard the regression-based estimate of the "observed" quantity as its "predicted" value. Thus, the remainder of this paper is using the term "prediction" in a statistical rather than hydrodynamic sense.

4.1 *Predictands*

The six predictands under consideration are bulk HMF's that quantify the portion of the total hydrometeor (condensate) mass contributed by each of the five hydrometeor classes (cloud water, cloud ice, rain, snow and hail) in a fully developed WISCDYMM-simulated storm, along with the total frozen hydrometeor mass, henceforth simply referred to as ice for brevity.

As in LWS05, SHW06 and SHW08, we compute each HMF by time-averaging the domain-integrated mass for the hydrometeor class in question over a large part of the mature storm stage and then dividing the result by the total domain-integrated condensate mass time-averaged over the same period. We denote the HMF's for cloud water, cloud ice, rain, snow, hail and ice by CWF, CIF, RF, SF, HF and IF respectively, where

$$IF = CIF + SF + HF.$$

We use 60-120 min as our time-averaging period, as also done in SHW06 and SHW08, because it spans a substantial fraction (50%) of the total simulation time and also begins long after the early (~15 min) bubble-induced overshooting updraft peak that occurs in most of the cases.

4.2 *Predictors*

For sole predictor of each HMF, our univariate linear regression analyses used one of the following three environmental indices derived from an upward probe of the processed initial sounding:

(1) The ground-relative melting level ZMLT. It is computed as the height AGL (above ground level, i.e., the lower boundary of the WISCDYMM domain) to which the base-state (ambient) temperature $T_0(z)$ interpolates linearly to 0˚C between the bottom and top of the lowest vertical grid interval in which its Celsius value changes sign from positive to negativei;

2) The cloud-base temperature TLCL. Equating cloud-base level with the lifting condensation level LCL, we compute TLCL from non-entraining parcel theory by launching the parcel from the ground and locating the level where the dry adiabat through the launching temperature intersects the dew point curve corresponding to the launching water vapor mixing ratio, defining parcel temperature and dew point profiles that are valid up to the LCL. As this intersection point must lie in the vertical grid interval where the resulting parcel dew point depression changes sign from positive at the bottom to negative at the top (before applying an instantaneous saturation adjustment to eliminate the supersaturation there), we locate the LCL by linearly interpolating the parcel dew point depression to zero, and finally compute TLCL by linearly interpolating the parcel temperature (prior to the adjustment) to the LCL;

3) The cloud-base pressure PLCL. It is computed by logarithmically interpolating the base-state pressure to the LCL in the same bracketing grid interval as for TLCL, invoking the standard assumption that the pressure in the parcel is in equilibrium with the environment at the same level.

Each of our bivariate linear regression analyses uses one of these three predictors jointly with CAPE, which is evaluated as

$$CAPE = g\int_{LFC}^{EL} \frac{T_p - T_0}{T_0} dz$$

where T_p is the parcel temperature, g is gravity [= 9.80 m s^{-2}], LFC is the level of free convection and EL the equilibrium level by the conventional definitions except that we set LFC = LCL in the unusual event that $T_p > T_0$ at the LCL. For initial soundings not modified by the low-level lifting mentioned in section 2, our CAPE values are typically ~20-50% larger than those computed on the University of Wyoming sounding archive. This is because we include latent heat of fusion when releasing latent heat to eliminate supersaturation where $T_p < 0$˚C, in full at -20˚C or colder and partially via a smooth transition from the liquid-only scenario between 0˚C and -20˚C, whereas the University of Wyoming ignores the latent heat of fusion. Our saturation vapor pressures transition from over liquid to over ice versus temperature in the same way as our latent heat coefficients.

Although the parcel is launched from the surface, its initial temperature and mixing ratio generally differ from the ambient (base-state) surface values, instead being based on adiabatic mixing of the lowest 500 m.

4.3 *Correlation parameters*

For univariate regression, let X denote the sole observed (WISCDYMM-derived) predictor, Z the observed predictand, and Z* the predicted (regression-derived) predictand. We focus on the following two correlation coefficients, computed after removing the mean values from all three quantities to simplify the calcutations as done by Panofsky and Brier (1958):

(a) r_{ZX}, the correlation between the observed *predictand* (one of the six HMF's) and the sole observed *predictor* (one of ZMLT, TLCL or PLCL), measuring how well their regression line fits the former versus the latter in their two-dimensional scattergram;

(b) r_{Z*Z}, the correlation between the univariately predicted *predictand* and the observed *predictand*, measuring how well the prediction under point (a) replicates the observations, a concept analogous to the so-called "A-B test" in audio engineering for comparing the sound quality of the output (the signal on a recording) versus the input (the program being recorded).

For bivariate regression, let X and Y denote the two observed (WISCDYMM-derived) predictors, again using Z to denote the observed predictand, and Z* the predicted (regression-derived) predictand. Analogously to the univariate scenario, we focus on the following two correlation coefficients, computed after removing the mean values from all four quantities:

(a#) R_{ZXY}, the multiple (or joint) correlation between the observed *predictand* (one of the six HMF's) and the two observed *predictors* (one of ZMLT, TLCL or PLCL, jointly with CAPE), measuring how well their regression plane fits the former versus the latter in their three-dimensional scattergram, defining R_{ZXY} to be the *non-negative* square root of the *squared* joint correlation coefficient R^2_{ZXY} in Panofsky and Brier (1958) because the only intrinsically *signed* correlation coefficients applicable to bivariate analysis are the simple (univariate) correlation coefficients r_{ZX}, r_{ZY} and r_{XY} that figure as follows

$$R^2_{ZXY} = \frac{r^2_{ZX} + r^2_{ZY} - 2r_{ZX}r_{ZY}r_{XY}}{1 - r^2_{XY}}$$

into computing R^2_{ZXY};

(b#) r_{Z*Z}, with the same meaning as under point (b) but now measuring the correlation between the *bivariately* predicted *predictand* and the observed *predictand*,

5. RESULTS

5.1 *Univariate and Bivariate Correlation Coefficients for "Observed" Hydrometeor Mass Fractions versus "Observed" Predictors*

Table 2 shows the univariate correlation coefficients, rounded to three decimal places, for all six HMF's versus each of the three primary predictors, together with the bivariate correlation coefficients similarly rounded for the same HMF's, jointly versus each primary predictor and CAPE, for all 105 WISCDYMM simulations. Table 3 displays the analogous correlation coefficients for the warm-month subset of 64. As noted in the Introduction, ZMLT both by itself and jointly with CAPE was also among the HMF predictors evaluated in SHW08, as shown in Tables 5 and 6 of the earlier paper for the full and warm-month storm populations respectively. Hence, the reprise of ZMLT as an HMF predictor in the current paper is intended not for sheer reiteration but as a benchmark against which to assess the skills of TLCL and PLCL.

Perusal of Tables 2 and 3 reveals that:

a) Except when predicting HF, TLCL as sole predictor produces appreciably stronger correlations than ZMLT, especially for SF. The improvement is academic for CWF, which is by far the weakest predictand. Jointly with CAPE, TLCL also produces a dramatic improvement versus using TLCL alone for each predictand except HF, for which the improvement is modest. Most encouragingly, the bivariate correlation magnitudes exceed 0.8 for IF, CIF and especially RF;

b) With the exceptions of SF and RF, PLCL as sole predictor further improves the predictands in comparison with TLCL, albeit only to a modest extent except more dramatically for CWF, which nevertheless remains the weakest predictand in the univariate regressions. However, adding CAPE as a joint predictor with PLCL produces far less improvement in the correlation magnitudes than when either ZMLT or TLCL is the primary predictor, and is of virtually no help in predicting either SF or RF. In fact, for three of the predictands (IF, HF, RF), the bivariate correlations themselves are lower for PLCL versus ZMLT as primary predictor;

c) These results are qualitatively similar for both the full set of storm cases (Table 2) and the warm-season subset (Table 3) despite some differences, mostly minor, in the precise magnitudes (to within the three decimal places displayed) of corresponding correlation coefficients.

The nature and scope of the findings just described call for three comments:

1) Much of the contrast, between the marked improvements from univariate to bivariate HMF predictions with ZMLT or TLCL as primary predictor and the much smaller improvements with PLCL as primary predictor, results from contrasting magnitudes among the correlations between each primary predictor and the secondary predictor, i.e., CAPE. These correlations (not tabulated) were sizable for ZMLT (0.461) and even more so TLCL (0.531) as primary predictor, but near zero (0.035) for PLCL. In the equation for R^2_{ZXY} at the end of section 4.3, the denominator shows that a sizable correlation between the two predictors (r_{XY}) tends to boost R^2_{ZXY} above r^2_{ZX} (and hence R_{ZXY} above $|r_{ZX}|$) more effectively than a smaller one, and that – in the worst-case scenario -- the second predictor is of no help if there is no correlation between the two predictors and also between the predictand and the secondary predictor;

2) The overall similarity between corresponding correlation coefficients, in Table 3 versus Table 2, is not surprising in light of Fig. 2. This diagram, identical to Fig. 4 of SHW08, illustrates one of the findings from SHW08 reviewed in the Introduction, namely the similarity between both the ranges and the mean values for the ice fraction IF in a given climatic zone with inclusion of the cool-month storm cases (left panel of Fig. 2) and without (right panel of Fig. 2), for the four best-sampled of the climate zones in Table 1 plus the "High Plains" cases. In view of these similarities, all further coverage of the results in sections 5.2 and 5.3 below pertains only to the full set of 105 cases;

3) In addition, in order to avoid an impractically large number of figures while highlighting some of our better results, the scope of our scattergram plots in these subsections is limited to just the ice fraction IF and rain fraction RF among the six predictands.

5.2 *Scattergrams for "Observed" Hydrometeor Mass Fractions versus Individual "Observed" Predictors*

A scattergram plot, including the regression line and correlation coefficient, is shown in Fig. 3 for the observed (WISCDYMM-derived) IF values versus ZMLT. Analogous scattergrams are shown in Figs. 4 and 5 for IF versus TLCL and PLCL respectively, and in Fig. 6 versus CAPE. Figures 3-5 all show substantial scatter, but the moderate improvement of the correlation coefficients in Fig. 4 and 5 over that in Fig. 3 is reflected in the more pronounced tapering of the scatter toward the lower end of the ranges for TLCL and PLCL in comparison with ZMLT. Figure 6 shows only a very weak positive correlation between IF and the secondary predictor CAPE. The poor correlation in Fig. 6 indicates that the large improvements from the univariate to the bivariate predictions of IF in Table 2 for ZMLT or TLCL as primary predictor are almost entirely due to the correlations between either of them and CAPE, in light of the equation for R^2_{ZXY}.

Analogous scattergrams to those for IF are plotted for RF in Figs. 7-10, which are otherwise the same as Figs. 3-6 in the same order. Although Table 2 and the corresponding numerical information in Figs. 7-9 show the RF has stronger correlations with each primary predictor than IF (albeit positive instead of negative), no importance can be attached to the apparently steeper regression lines in those diagrams versus Figs. 3-5 because the vertical scales in Figs. 7-9 are stretched twofold to fill out most of the vertical extent of the plot with the generally smaller values of RF versus IF, Figure 10 shows only a tiny negative correlation between RF and CAPE, much weaker yet than the small positive correlation between IF and CAPE in Fig. 6, so the deduction about the main cause of the superior bivariate versus univariate predictions of IF holds even more strongly for RF.

5.3 *Scattergrams for "Predicted" versus "Observed" Hydrometeor Mass Fractions*

Figure 11 superimposes two scattergrams and the associated regression lines for the *predicted* versus *observed* values of the predict*and* IF, one for the univariate prediction versus ZMLT (red triangles and regression line) and the other for the bivariate prediction versus ZMLT and CAPE (black dots and regression line), also showing the correlation coefficients for both scattergrams. Figures 12 and 13 do likewise, but using TLCL and PLCL respectively as the primary predictor instead of ZMLT. Analogous plots to Figs. 11-13, but for RF instead of IF, are shown in Figs. 14-16.

The mode of plotting in Figs. 11-13 and Figs. 14-16 differs fundamentally from Figs. 3-5 and Figs. 7-9 respectively. In the previous plots the points represent the *observed* predict*and* versus the observed predict*or*. But now, the intent is to use two scattergrams in a single diagram to gauge how well the predictions (the regression analyses whose correlation coefficients are displayed in Table 2) replicate the observations (the output from WISCDYMM) for the predict*and* in both the univariate and bivariate frameworks, as intimated in section 4.3. As the ideal standard against which to compare both scatter patterns, the blue diagonal line in each of Figs. 11-16 represents a perfect prediction, with a correlation coefficient of unity.

As a bonus, this approach avoids the awkward visual issues inherent in using a flat medium to try displaying a bivariate regression fit in predictand-versus-predictors mode. Conceptually, bivariate regression entails a three-dimensional scattergram and associated regression plane, but on a flat medium the best that one can do is a two-dimensional projection of such a display, collapsing much of the perspective.

In each of Figs. 11-16, one salient feature is that the correlation coefficients for the predicted versus observed values of the predictand have the same magnitudes as for the observed predictand versus the predictor(s), for both the univariate and bivariate predictions. This equality of magnitudes is not coincidental, and turns out to be valid for any combination of predictand Z and sole predictor X in univariate analysis, i.e.,

$$r_{Z^*Z} = |r_{ZX}|$$

as well as any combination of predictand Z and two predictors X and Y in bivariate analysis, i.e.,

$$r^2_{Z^*Z} = R^2_{ZXY}$$

The proofs of these equalities are omitted here. In short, they entaill invoking the equations for the regression line in the univariate prediction, or the regression plane in the bivariate prediction, with all mean values subtracted out as in Panofsky and Brier (1958), and from there deriving the equalities via some algebra, easily in the former case and much more laboriously in the latter.

With ZMLT or TLCL as primary predictor, the improved quality of the bivariate predictions over their univariate counterparts is evident in Figs. 11-12 for IF, and in Figs. 14-15 for RF. In each of these diagrams, the distribution of points shifts so as to appreciably ameliorate the obvious univariate limitations of overpredicting the observed HMF toward the low end of its distribution and underpredicting it toward the high end. These benefits are, of course, also reflected in the steeper regression line for the bivariate versus univariate fit, tilting it closer to the blue perfect-prediction line even though the scatter is not dramatically lessened. In Figs. 14-15, many of the overpredicted rain fractions extend into the lower midrange, which is also improved in the bivariate prediction. Outliers may not be improved, however, as exemplified by the two smallest observed rain fractions in Fig. 15; the univariate regression underpredicts them, and the bivariate regression worsens their underprediction.

In the two figures with PLCL as primary predictor, Fig. 13 for IF and Fig. 16 for RF, the meagerness of the improvement for bivariate versus univariate regression is starkly evident, especially in the latter plot where the impact is all but nonexistent. Both figures show very little steepening of the regression line and correspondingly little shift of the point distribution. The lower half of the IF spread in Fig. 13 is grossly overpredicted, especially toward the end, while Fig. 16 shows overprediction of most low-end and many midrange RF values with gross underprediction of high-end values. Though all four correlation coefficients in Figs. 13 and 16 are near or somewhat above 0.6 and thus far from trifling, these two figures serve as a caveat that substantial prediction errors over a major portion of a predictand's range can still lurk behind an ostensibly respectable linear correlation.

6. CONCLUSIONS

1) As a sole predictor of HMF's among the six indices under consideration, TLCL performs considerably better ZMLT, except when predicting hail.

2) TLCL is also dramatically superior jointly with CAPE than alone, for each predictand except hail, performing especially well for rain and only slightly less so for cloud ice and total ice.

3) Except for snow and rain, PLCL is slightly better yet as sole predictor than TLCL.

4) However, PLCL is far less superior as a joint predictor with CAPE than it is alone, unlike for either ZMLT or TLCL as the primary predictor, and barely at all when predicting rain or snow. This ineffectiveness springs largely from a near-zero correlation between CAPE and PLCL, versus a solidly fair correlation between CAPE and each of the other two primary predictors.

5) In fact, the bivariate skill indices are *lower* for PLCL versus ZMLT as the primary predictor for three of the six HMF's (rain, hail, total ice).

6) The results are qualitatively similar for the warm-season subset of the WISCDYMM storm simulations versus the full set despite some differences, mostly minor, in the precise magnitudes of corresponding correlation coefficients.

7. ACKNOWLEDGMENTS

The thunderstorm simulations reported herein are based on research partially supported by National Science Foundation (NSF) Grants ATM-0234744 and ATM-0244505. Any findings or opinions expressed in this paper are those of the authors and do not necessarily reflect the views of NSF.

For the suggestion of repeating our univariate and bivariate regression analyses in SHW08 using the

cloud-base temperature and cloud-base pressure as alternative primary predictors to the melting level, we thank an anonymous reviewer of our first attempt at submitting the material in SHW08 to a journal for formal publication.

8. REFERENCES

Cotton, W. R., M. A. Stevens, T. Nehrkorn, and G. J. Tripoli, 1982: The Colorado State University three-dimensional cloud/mesoscale model - 1982. Part II: An ice phase parameterization. *J. Rech. Atmos*., **16**, 295-320.

______, G. J. Tripoli, R. M. Rauber, and E. A.. Mulvihill, 1986: Numerical simulations of the effects of varying ice crystal nucleation rates and aggregation processes on orographic snowfall. *J. Clim. Appl. Meteor*., **25**, 1658-1680.

Johnson, D. E., P. K. Wang, and J. M. Straka, 1993: Numerical simulations of the 2 August 1981 CCOPE supercell storm with and without ice microphysics. *J. Appl. Meteor*., **32**, 745-759.

______, ______, and ______, 1994: A study of microphysical processes in the 2 August 1981 CCOPE supercell storm. *Atmos. Res*., **33**, 93-123.

Klemp, J. B., and R. B. Wilhelmson, 1978: The simulation of three-dimensional convective storm dynamics. *J. Atmos. Sci*., **35**, 1070-1096.

Lin, H.-M., and P. K. Wang, 1997: A numerical study of microphysical processes in the 21 June 1991 northern Taiwan mesoscale precipitation system. *Terr. Atmos. Ocean. Sci*., **4**, 385-404.

______, ______, and R. E. Schlesinger, 2005: Three-dimensional nonhydrostatic simulations of summer thunderstorms in the humid subtropics versus High Plains. *Atmos. Res*., **78**, 103-145.

Lin, Y.-L., R. D. Farley, and H. D. Orville, 1983: Bulk parameterization of the snow field in a cloud model. *J. Clim. Appl. Meteor*., **22**, 1065-1092.

Moran, J. M., and M. D. Morgan, 1994: *Meteorology: The Atmosphere and the Science of Weather*, 4th ed. Macmillan College Publishing Company, New York, 517 pp.

Panofsky, H. A., and G. W. Brier, 1958: *Some Applications of Statistics in Meteorology*, 1st ed. The Pennsylvania State University, University Park, 224 pp.

Schlesinger, R. E., S. A. Hubbard, and P. K. Wang, 2006: A three-dimensional cloud modeling study of the dynamical and microphysical variability of thunderstorms in different climate regimes. *Preprints 12th Conf. Cloud Physics*, Madison, WI, Amer. Meteor. Soc., Boston, MA, Paper 8.6 (CD-ROM).

______, ______, and ______, 2008: Worldwide jmicrophysical thunderstorm variability in different climatic regions: A three-dimensional cloud modeling study. *Preprints 24th Conf. Severe Local Storms*, Savannah, GA, Amer. Meteor. Soc., Boston, MA, Paper 17B5 (Web page: ams.confex.com/ams/pdfpapers/142204.pdf).

Straka, J. M., 1989: Hail growth in a highly glaciated central High Plains multi-cellular hailstorm. Ph.D. thesis, University of Wisconsin – Madison, 413 pp.

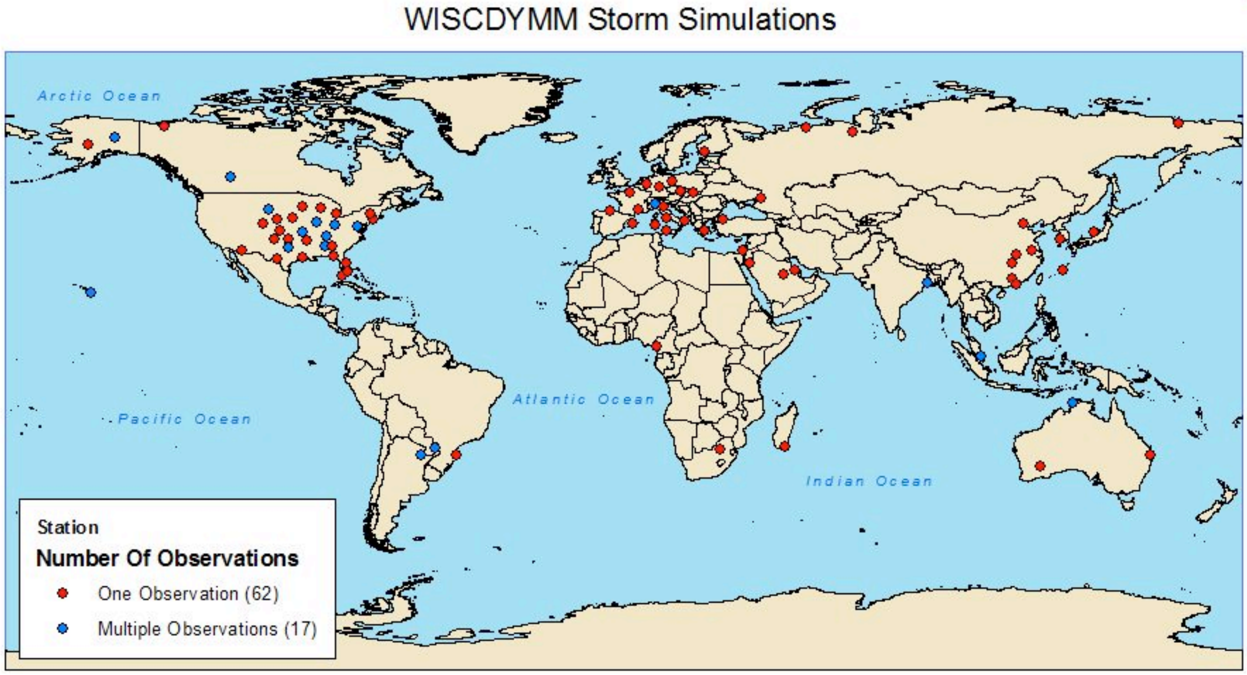

Fig. 1. Global map projection marking the locations of the 79 rawinsounding stations listed in Table 1 of SHW08, using red dots to represent the 62 stations associated with one thunderstorm case and blue dots to represent the 17 stations associated with multiple cases.

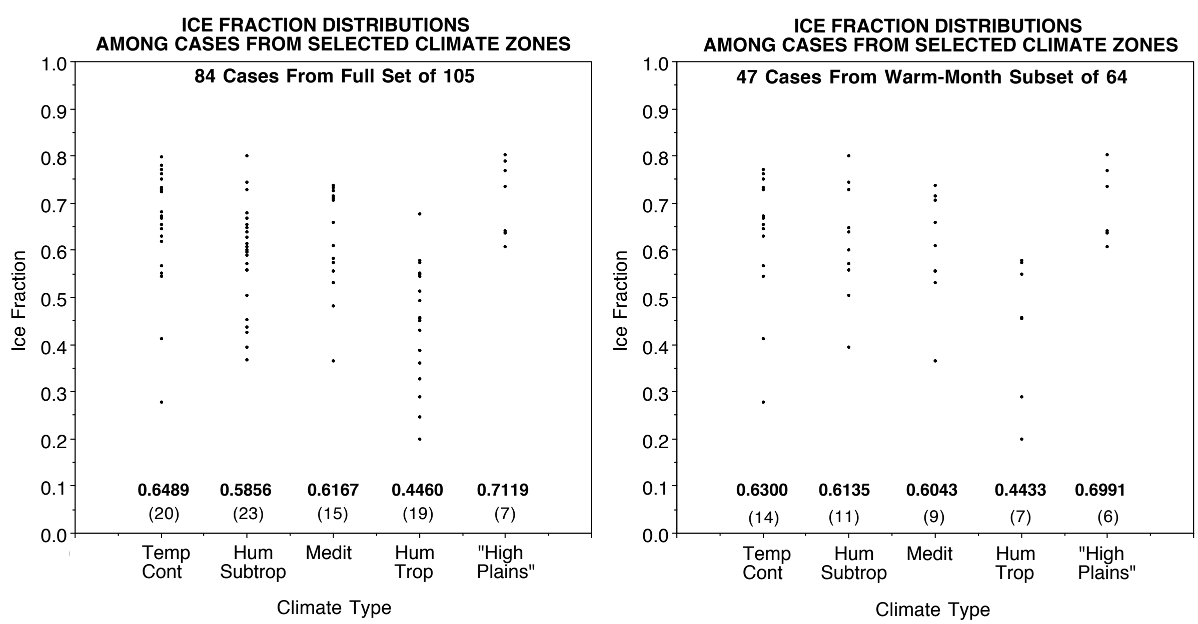

Fig. 2. Distributions of 60-120 min time-averaged ice fractions for the simulated thunderstorms from the four best-sampled climate zones [temperate continental with warm summers (Temp Cont), humid subtropical (Hum Subtrop), Mediterranean (Medit) and humid tropical (Hum Trop)] plus the “High Plains” stations in the dry/steppe and boreal climate zones. Just above the bottom of a panel, each bold-faced number is the mean ice fraction for all cases in the corresponding category, and the number of cases in that category is shown in parentheses underneath. Left panel: 84 cases from the full set of 105. Right panel: 47 cases from the warm-season subset of 64.

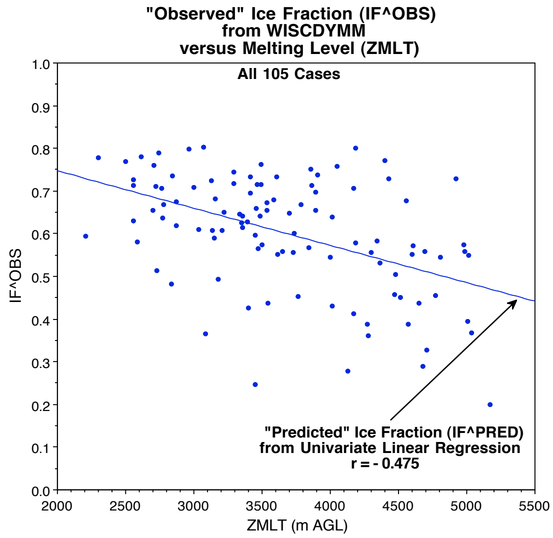

Fig. 3. Scattergram and least-squares regression line with corresponding correlation coefficient r for "observed" (WISCDYMM-generated) ice fraction IF as predictand versus ground-relative melting level ZMLT as predictor, for all 105 thunderstorm cases.

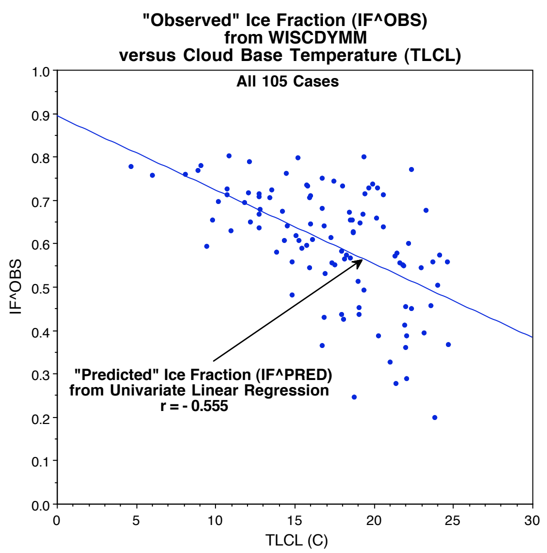

Fig. 4. Same as Fig. 3, but for cloud-base temperature (TLCL) as predictor.

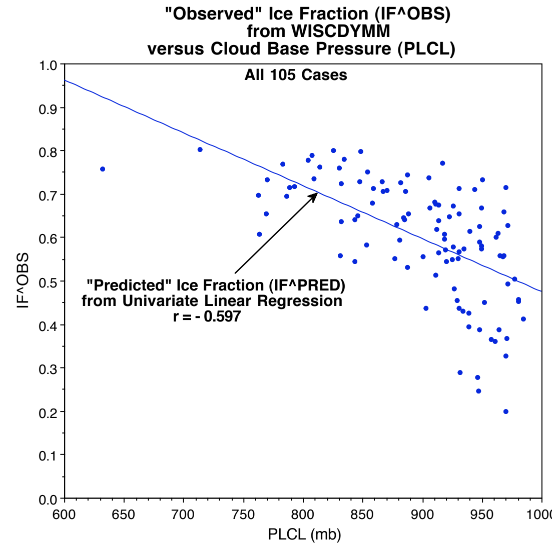

Fig. 5. Same as Fig. 3, but for cloud-base pressure (PLCL) as predictor.

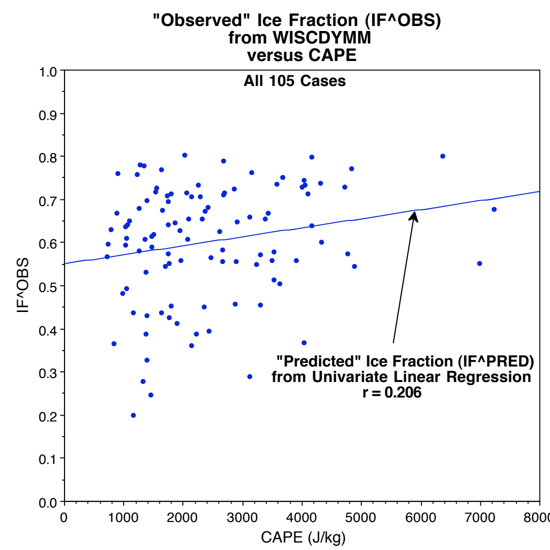

Fig. 6. Same as Fig. 3, but for CAPE as predictor.

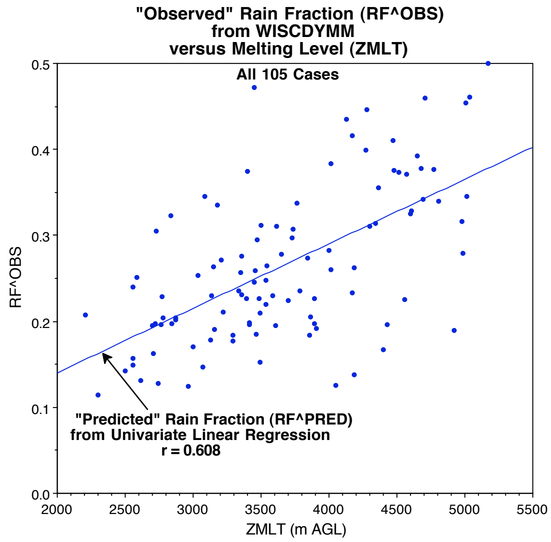

Fig. 7. Same as Fig. 3, but for “observed” (WISCDYMM-generated) rain fraction RF as predictand instead of IF.

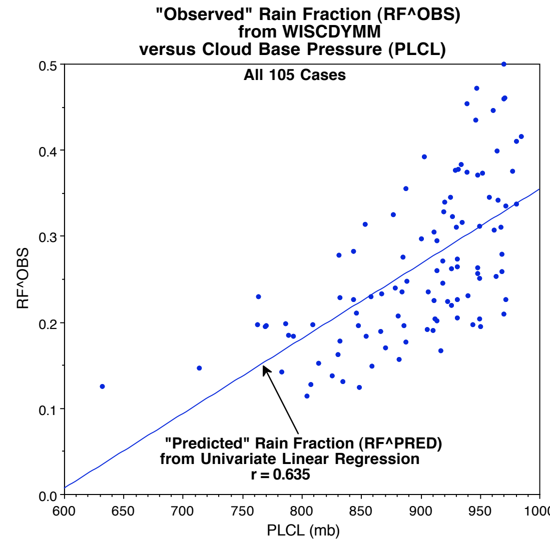

Fig. 9. Same as Fig. 5, but for “observed” (WISCDYMM-generated) rain fraction RF as predictand instead of IF.

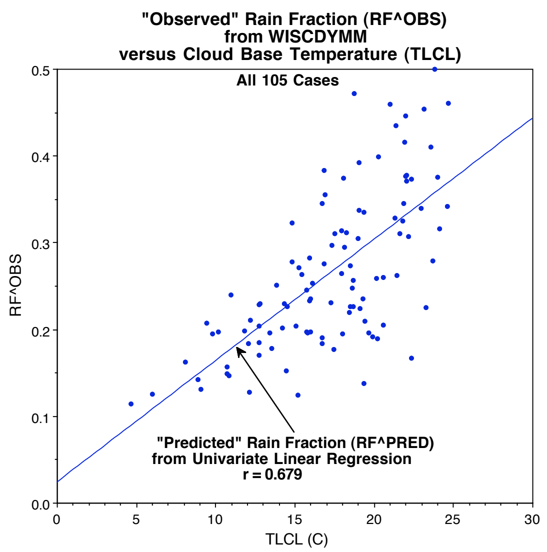

Fig. 8. Same as Fig. 4, but for “observed” (WISCDYMM-generated) rain fraction RF as predictand instead of IF.

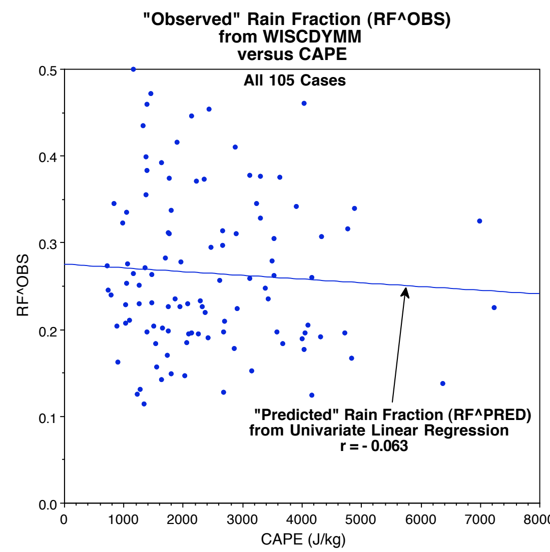

Fig. 10. Same as Fig. 6, but for “observed” (WISCDYMM-generated) rain fraction RF as predictand instead of IF.

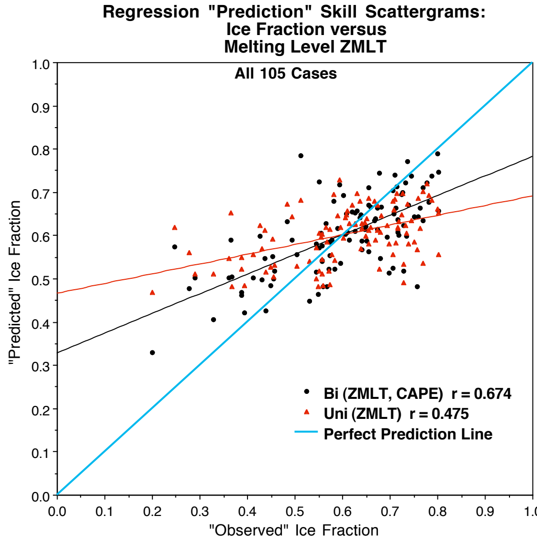

Fig. 11. Scattergrams and least-squares regression lines with corresponding correlation coefficients (r), for "predicted" (linearly regressed) versus "observed" (WISCDYMM-generated) ice fraction IF, for all 105 thunderstorm cases. Triangles and regression line in red represent results from univariate "prediction" of IF versus ground-relative melting level ZMLT, while dots and regression line in black represent results from bivariate "prediction" of IF versus ZMLT and CAPE. Blue diagonal line represents a perfect prediction with r = 1.00.

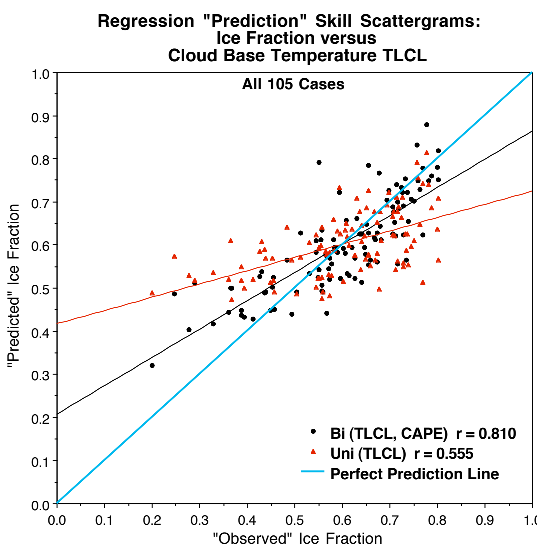

Fig. 12. Same as Fig. 11, but for cloud-base temperature TLCL instead of ZMLT.

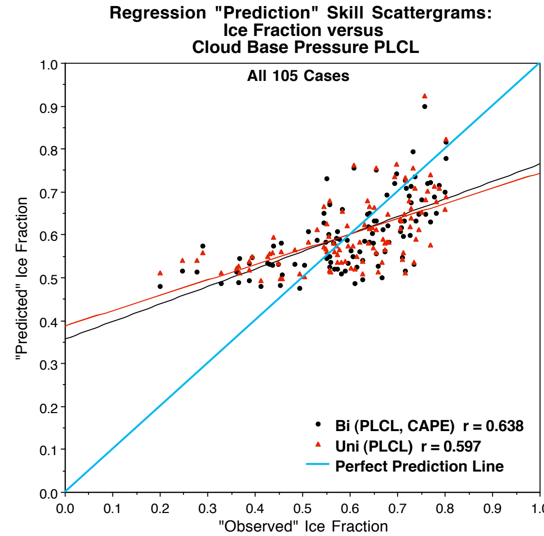

Fig. 13. Same as Fig. 11, but for cloud-base pressure PLCL instead of ZMLT.

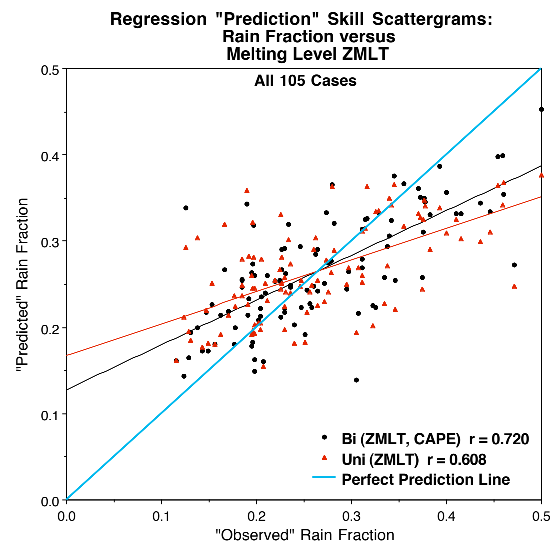

Fig. 14. Same as Fig. 11, but for rain fraction RF instead of IF.

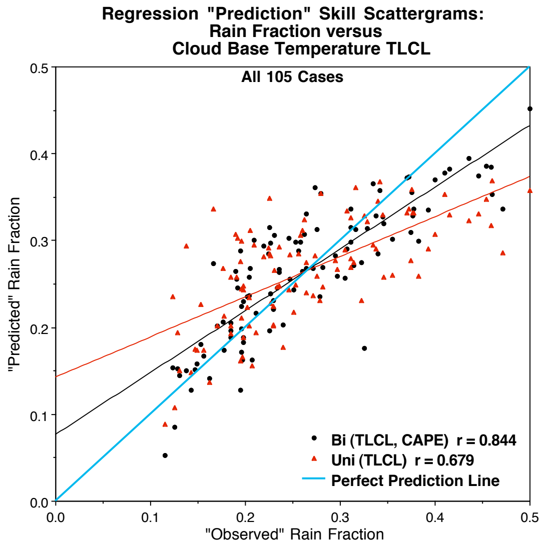

Fig. 15. Same as Fig. 12, but for rain fraction RF instead of IF.

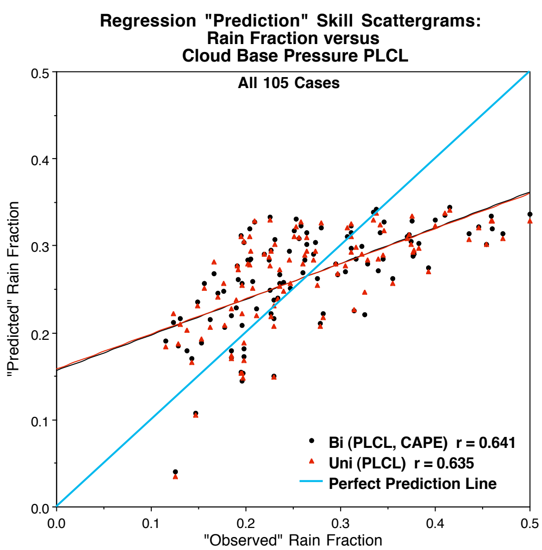

Fig. 16. Same as Fig. 13, but for rain fraction RF instead of IF.

Table 1. Breakdown of counts for the 79 rawinsounding stations and 105 thunderstorm cases in Table 1 of SHW08 among the 10 climatic zones listed therein.

Climatic zone	Number of stations	Number of cases
Temperate continental, warm summer	13	20
Humid subtropical	16	23
Mediterranean	13	15
Humid tropical	12	19
Temperate continental, cool summer	4	4
Dry/steppe	7	8
Boreal	3	5
Polar, tundra	4	4
Temperate oceanic	3	3
Dry/desert	4	4

Table 2. Linear correlation coefficients between selected 60-120 min time-averaged domain-integrated hydrometeor mass fractions as predictands and selected initial environmental indices as predictors, using abbreviations explained in the text, for the full set of 105 worldwide thunderstorm simulations.

	Predictand					
Predictor(s)	**IF**	**CIF**	**HF**	**SF**	**CWF**	**RF**
ZMLT	-0.475	-0.458	-0.408	-0.328	+0.159	+0.608
ZMLT, CAPE*	0.674	0.648	0.599	0.434	0.542	0.720
TLCL	-0.555	-0.576	-0.397	-0.510	+0.235	+0.679
TLCL, CAPE*	0.810	0.826	0.628	0.673	0.647	0.844
PLCL	-0.597	-0.613	-0.453	-0.507	+0.405	+0.635
PLCL, CAPE*	0.638	0.650	0.502	0.520	0.569	0.641

*Versus multiple predictors, correlation coefficients possess magnitude but no sign.

Table 3. Same as Table 2, except for the subset of 64 worldwide thunderstorm simulations for warm months only.

	Predictand					
Predictor(s)	**IF**	**CIF**	**HF**	**SF**	**CWF**	**RF**
ZMLT	-0.454	-0.440	-0.336	-0.405	+0.132	+0.602
ZMLT, CAPE*	0.691	0.638	0.654	0.444	0.572	0.723
TLCL	-0.535	-0.554	-0.320	-0.596	+0.178	+0.694
TLCL, CAPE*	0.852	0.832	0.701	0.705	0.666	0.891
PLCL	-0.601	-0.621	-0.452	-0.518	+0.348	+0.673
PLCL, CAPE*	0.683	0.682	0.601	0.519	0.591	0.691

*Versus multiple predictors, correlation coefficients possess magnitude but no sign.